Solar Energy 184 (2019) 292–304

Contents lists available at ScienceDirect

Solar Energy

journal homepage: www.elsevier.com/locate/solener

An improved and comprehensive mathematical model for solar photovoltaic modules under real operating conditions

Tao Ma*, Wenbo Gu, Lu Shen, Meng Li

School of Mechanical Engineering, Shanghai Jiao Tong University, Shanghai, China

ARTICLE INFO

Keywords:
Solar photovoltaic
Mathematical model
PV simulation
Performance evaluations

ABSTRACT

This paper presents an improved and comprehensive mathematical model for photovoltaic (PV) device, developed in Matlab based on the basic circuit equation of a solar cell with the basic data provided by the manufacturer. The effects of solar radiation, ambient temperature and cell types, including monocrystalline and polycrystalline silicon are fully considered. First, based on the developed model, the characteristics of two types of PV modules has been obtained and verified by other widely used models. Results show that the model can produce the characteristic curves quickly and accurately because initial values assumption and multiple iterations can be avoided. This model is further validated through comparisons between simulated and the measured curves from a real PV system, and very good agreement is achieved between each other, with relative errors at 0.43% and 0.36% for two types of PV. Finally, this model is employed to simulate the performance of a PV system under actual typical cases. The relative error between the simulated and measured electricity on a sunny and cloudy day is 0.60% and −1.08%, respectively, demonstrating the effectiveness of the proposed method.

1. Introduction

Nowadays renewable energy becomes an essential role in the world energy market day by day due to global warming problem and serious air pollution from the burning of fossil fuels (Kumar et al., 2015). The demand for renewable energy grows sharply around the world, especially solar energy because of its wide distribution, abundance, and cleanness (Alam et al., 2015; Awadallah, 2016; Kittisontirak et al., 2016). Photovoltaic (PV) power generation is a common way to make use of solar energy, using solar cells to convert solar energy directly into electric energy through PV effect.

Now the global total PV installation capacity is about 405 GW, while China is leading the PV market with a total installation of 130 GW until 2017 (Junnan et al., 2018). Estimation of PV power output becomes more important than ever for a rapid PV system design (Arefifar et al., 2017; Shen et al., 2018; Watson et al., 2018). However, the power output of PV modules is greatly affected by the actual external environment, such as, solar radiation (Bana and Saini, 2016; Marco Tina, 2016), temperature (Bahaidarah et al., 2016; Gökmen et al., 2016; Reddy et al., 2015), soiling (Appels et al., 2013; Kimber et al., 2007; Mejia and Kleissl, 2013; Urrejola et al., 2016), shading (Sun et al., 2012; Wang et al., 2011), etc. Also, these various weather parameters can deteriorate the performance of PV modules because of aging loss during its lifetime (Azizi et al., 2018; Doumane et al., 2015). It is inaccessible to get the real power from product suppliers because the specifications provided by the manufacturer are obtained under two special conditions. One is the standard test conditions (STC), i.e. solar irradiance $G = 1000\,W/m^2$, cell temperature $T_c = 25\,^{\circ}C$ and air mass $AM = 1.5$, and the other one is the nominal operating cell temperature (NOCT) conditions. Both of them are very different from real operation conditions (Marco Tina, 2016). Even when the solar intensity and ambient temperature are constant, the PV module can still output different voltages, only at a certain output voltage value, the output power of the component can reach the maximum value. Therefore, in order to improve PV power output, the operating point of the PV module should be adjusted in real time so that it always works at the maximum power point, which means that acquiring the output characteristics of the PV module is essential. If the actual measurement of the PV module is made directly, specific environmental conditions are required, and high experimental costs are also incurred since the output characteristics of the component are highly dependent on natural climatic conditions. Therefore, if the output characteristics and maximum power output of the PV module under different illumination and temperature can be predicted only using the manufacturer's data, masses of experimental costs and time will be saved (Tossa et al., 2018).

Modeling and simulation is essential to assess the output

* Corresponding author.
E-mail address: tao.ma@connect.polyu.hk (T. Ma).

https://doi.org/10.1016/j.solener.2019.03.089
Received 25 December 2018; Received in revised form 15 March 2019; Accepted 26 March 2019

Nomenclature

Abbreviations

IQR	interquartile range
I-V	current-voltage
MBE	mean bias error
MPP	maximum power point
PV	photovoltaic
P-V	power-voltage
RMSE	root mean square error
SOC	state of charge
STC	standard test conditions

Symbols

C	temperature coefficient (A/K^3)
E_g	band gap (eV)
G	solar radiation (W/m^2)
I_{mp}	current at maximum power point (A)
I_0	saturation current of a diode (A)
I_{ph}	light-generated current (A)
I_{sc}	short-circuit current (A)
K	Boltzmann's constant (1.381E − 23 J/K)
n	ideality factor of diode
N_s	number of cells in series in one module
P_{max}	maximum power (W)
q	electric charge (1.602E − 19C)
R^2	coefficient of determination
R_p	module parallel resistance (Ω)
R_{pc}	parallel resistance of the solar cell (Ω)
R_s	module series resistance (Ω)
R_{sc}	series resistance of the solar cell (Ω)
T_a	ambient temperature (K)
T_c	temperature of a solar cell (K)
T_{NOCT}	nominal operating cell temperature (°C)
V_{mp}	voltage at maximum power point (V)
V_{oc}	open-circuit voltage (V)
V_t	diode thermal voltage (V)

Subscripts

ref	reference conditions, i.e. standard test conditions

Greek symbols

α	temperature coefficient of short circuit current under standard test conditions (%/°C)
β	temperature coefficient of open-circuit voltage under standard test conditions (V/°C)
γ	temperature coefficient of maximum power under standard test conditions (%/°C)

characteristics and energy production of solar cells under general meteorological conditions. PV cell model is the most important part of any PV simulation (Goe and Gaustad, 2015). It is always desirable to develop a model which can closely get the characteristics of physical solar cells, i.e. fits the measured current-voltage (*I-V*) data under real operation conditions (Ding et al., 2016; Lim et al., 2015). The most popular modelling approach is to take the electrical equivalent circuit into the system design, which is made up of both linear and non-linear components (Chin et al., 2015). In recent decades, substantial study has been conducted to particularly obtain the circuit variables, such as the photocurrent (I_{ph}), saturation current (I_0), diode ideality factors (n), series resistance (R_s) and parallel resistance (R_p) in the electrical equivalent circuit for PV design (Bouraiou et al., 2015; Chen and Huang, 2016; Vimalarani and Kamaraj, 2015). Among them, one simple model is denoted as ideal model without considering the internal losses of the current (3-parameter model), and the one-diode model, also called 4-parameter model, takes account only series resistance with neglecting the parallel resistance (Jordehi, 2016). In literature, Walker (2014) employed the 4-parameter model to calculate related parameters and show how the maximum power point varies with temperature and solar radiation. Krismadinata et al. (2013) described a novel method to set the 4-parameter model, and the simulation results can agree well with the datasheets for different types of PV modules. The same assumption considering the parallel resistance too large to be neglected was adopted in Ref. (Babu, 2012; Celik and Acikgoz, 2007; Khatib et al., 2013; Kou et al., 1998), with simulation models implemented in Simulink/Matlab. Although the results show that the simulation blocks were similar to real PV modules, there is still an apparent gap between the simulation and the experiment results when current follows with temperature due to temperature effect (Celik and Acikgoz, 2007).

To improve the simulation accuracy as much as possible, the two-diode model which consists of two diodes, series resistance and parallel resistance was proposed in the field of PV simulation. It is also called 7-parameter model, because it requires to solve seven parameters. The two-diode model is known to have a unique advantage of describing some special PV types, such as thin films, etc. (Chin et al., 2016) and the PV cells under extraordinary weather conditions, like low irradiance level (Ishaque et al., 2011b). Ishaque et al. (2011a) simplified seven unknown parameters into four pending parameters including I_{ph}, I_0, R_s, R_p with some assumptions to reduce computation time. The formal two parameters can attain analytically and the latter two parameters can obtain by iteration. Dehghanzadeh et al. (2017) adopted Thevenin's theorem and a piecewise linear model to transform the nonlinear and implicit equation into the explicit model, and then the applicability of the model was fully examined through simulation, experiment and circuit analysis. Yordanov et al. (2012) employed the method of series resistance corrected local ideality factor versus current to take place of *I-V* data analysis for c-Si PV modules based on experiment results for avoiding difficult computational procedures including non-linear curve fitting. Moreover, substantial work has been conducted for the two-diode model to extract these parameters as simple as possible (Babu and Gurjar, 2014; Chin et al., 2016; Ma et al., 2014d). However, the two-diode model is quite complicated, time-consuming and might be unable to converge since it involves two exponential terms and seven pending parameters in a nonlinear and non-explicit equation (Ma et al., 2014c).

To balance the accuracy and complexity of PV simulation model, the one-diode model considering both R_s and R_p was put forward (Tossa et al., 2014). It is also called 5-parameter model, which consists of photocurrent, saturation current, diode ideality factors, series resistance and shunt resistance (Chaibi et al., 2018). De Soto et al. (2006) applied the four equations at three particular points and the equation of temperature coefficient to determine the five parameters and validated the model by experiment while the ideality factor calculated from this model was usually less than one, not within the reasonable range. Tian et al. (2012) revealed a modified *I-V* relationship for the single-diode model and performed a series of outdoor experiments for a PV array with various specifications to validate the model. Our previous study (Ma et al., 2014b) employed six nonlinear equations to determine the five parameters of a PV device and validated the simulated results from a slightly modified model by field measurement, offering a very good compromise between accuracy and simplicity. Lots of similar work has been done in literature (Ayodele et al., 2016; Bai et al., 2014; Ibrahim and Anani, 2017), while in these models complex computer codes are

required to be programmed at first and then the five parameters should be determined by calculating numerous functions and iterating dozens of times, even hundreds of times after selecting constantly proper initial value in a reasonable range, and even sometimes the determination method of the model may not be converged because of rough initial values and unusual physical parameters under special weather conditions.

In this study, a comprehensive 5-parameter PV simulation model is developed based on our previous work in PV modelling (Ma et al., 2014b). In the improved model, there is no need to iterate the complicated equations and determine complex initial values as usual. Except for the basic available manufacturer template data, there is also no need for any other information as well, unlike other complicated models which may make use of experimental data (Bellia et al., 2014). The solutions of the four parameters are analytically obtained and the remaining one can be easily determined by 'fzero' function considering the effect of solar radiation and temperature in Matlab. The developed model can fit different types of panels well and various weather conditions.

The remaining part of the paper is organized as follows. Section 2 provides a comprehensive mathematical model and determination procedures, and then validated in Section 4. The model is also employed in Section 4 to predict power output of real PV systems and examine its application. Finally the whole study is summarized in Section 5.

2. Mathematical model

A PV module is made up of many solar cells connected in series or in parallel. The common technique of modeling a solar cell is to develop an equivalent circuit based on the 5-parameter model, which is composed of a current source, a diode, a parallel resistance (R_{pc}) and a series resistance (R_{sc}) The one-diode PV mathematical model can be represented by Eq. (1) (Celik and Acikgoz, 2007; Kou et al., 1998), and its equivalent circuit is shown in Fig. 1.

$$I = I_{ph} - I_d - I_p = I_{ph} - I_0\left[\exp\left(\frac{V + I\cdot R_{sc}}{V_t}\right) - 1\right] - \frac{V + R_{sc}I}{R_{pc}} \tag{1}$$

where I_{ph} is the light-generated current (A), I_0 is the reserve saturation current of the diode (A), R_{sc} is the series resistance of the solar cell (Ω), R_{pc} is the parallel resistance of the solar cell (Ω), $V_t = n{\cdot}K{\cdot}T_c/q$ is the diode thermal voltage (V), n is the diode ideality factor, q is the charge of the electron (1.602E−19C), K is the Boltzmann's constant (1.381E−23 J/K) and T_c is the temperature of solar cell (K).

When many solar cells are connected in series to form a PV module. The output current I and output voltage V of the module have the relationship according to Eq. (2) (Tian et al., 2012).

$$\begin{aligned} I &= I_{ph} - I_0\left[\exp\left(\tfrac{1}{V_t}(\tfrac{V}{N_s} + I\cdot R_{sc})\right) - 1\right] - \tfrac{1}{R_{pc}}\left(\tfrac{V}{N_s} + R_{sc}I\right) \\ &= I_{ph} - I_0\left[\exp\left(\tfrac{V + I\cdot R_s}{N_s V_t}\right) - 1\right] - \tfrac{V + R_s I}{R_p} \end{aligned} \tag{2}$$

where $R_s = N_s{\cdot}R_{sc}$ is module series resistance (Ω), $R_p = N_s{\cdot}R_{pc}$ is module parallel resistance (Ω) and N_s is the number of cells in series in one module.

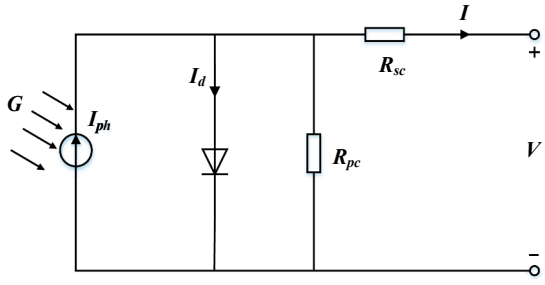

Fig. 1. Equivalent circuit for a solar cell.

The monocrystalline silicon SQ175-PC from Shell Solar and polycrystalline silicon STP200-18/Ub-1 from Suntech are used as samples in the present study. The key parameters of SQ175-PC and STP200-18/Ub-1 PV modules provided by manufacturer are listed in Table 1, which have been reported in our previous study (Ma et al., 2013; Ma et al., 2014a,c; Ma et al., 2016).

3. Parameters analysis

3.1. Parameters analysis at standard test conditions

Because key parameters under STC and T_{NOCT} are provided by the manufacturer, it is necessary to set up the model at STC. As known, Eq. (3) can be deduced:

$$I = I_{ph,ref} - I_{0,ref}\left[\exp\left(\frac{V + I\cdot R_{s,ref}}{N_s V_{t,ref}}\right) - 1\right] - \frac{V + R_{s,ref}I}{R_{p,ref}} \tag{3}$$

The subscript 'ref' refers to the related parameters under STC.

Therefore, the five parameters in Eq. (3) should be determined: $I_{ph,ref}$, $I_{0,ref}$, $R_{p,ref}$, $R_{s,ref}$ and $V_{t,ref}$.

3.1.1. The diode thermal voltage V_t at STC

The parallel resistance is usually very large when compared to series resistance. Therefore, Eq. (3) can be simplified as Eq. (4).

$$I = I_{ph,ref} - I_{0,ref}\left[\exp\left(\frac{V + I\cdot R_{s,ref}}{N_s V_{t,ref}}\right) - 1\right] \tag{4}$$

At the open circuit voltage point (V_{oc}, 0): $I = 0$, $V = V_{oc,ref}$, which can be taken into the Eq. (4), therefore:

$$0 = I_{ph,ref} - I_{0,ref}(\exp(\frac{V_{oc,ref}}{N_s V_{t,ref}}) - 1) \approx I_{ph,ref} - I_{0,ref}\exp(\frac{V_{oc,ref}}{N_s V_{t,ref}}) \tag{5}$$

Because the exponential part exp ($V_{oc,ref}$ /$N_s V_{t,ref}$) is much greater than 1, the equation can be simplified as Eq. (5) and it can be rewritten as:

$$V_{oc,ref} \approx -N_s V_{t,ref}\ln(\frac{I_{0,ref}}{I_{ph,ref}}) \tag{6}$$

For the temperature coefficient of voltage,

$$\beta = \frac{\mathrm{d}V_{oc,ref}}{\mathrm{d}T} = \frac{\mathrm{d}}{\mathrm{d}T}[N_s V_{t,ref}\ln I_{ph,ref} - N_s V_{t,ref}\ln I_{0,ref}] \tag{7}$$

Therefore,

$$\beta = \frac{N_s V_{t,ref}}{T_{ref}}\ln(\frac{I_{ph,ref}}{I_{0,ref}}) + N_s V_{t,ref}\left[\frac{1}{I_{ph,ref}}\frac{\mathrm{d}I_{ph,ref}}{\mathrm{d}T} - \frac{1}{I_{0,ref}}\frac{\mathrm{d}I_{0,ref}}{\mathrm{d}T}\right] \tag{8}$$

As known, the diode saturation current is proportional to the cube of temperature (Silva, 2013), which is expressed as:

$$I_{0,ref} = CT_{ref}^3\exp(-\frac{qE_g}{KT_{ref}}) \tag{9}$$

where C is temperature coefficient (A/K^3), E_g is the band gap in eV, which depends on the PV cell technology and its value is available in De Soto et al. (2006) for different cell types. Besides, E_g is also affected by the cell temperature, while the temperature could be neglected and it would not cause a significant error (Navabi et al., 2015). Therefore, E_g is chosen as 1.121 eV for monocrystalline silicon and polycrystalline silicon.

So

$$\beta = \frac{N_s V_{t,ref}}{T_{ref}}\ln(\frac{I_{ph,ref}}{I_{0,ref}}) + N_s V_{t,ref}\left[\frac{\alpha}{I_{ph,ref}} - \frac{3}{T_{ref}} - \frac{qE_g}{KT_{ref}^2}\right] \tag{10}$$

Table 1
PV module key parameters.

Specification	SQ175-PC	STP200-18/Ub-1
Cell type	Monocrystalline	Polycrystalline
Open-Circuit Voltage at STC ($V_{oc,ref}$)	44.6 V	33.4 V
Short-Circuit Current at STC ($I_{sc,ref}$)	5.43 A	8.12 A
Voltage at maximum power point at STC ($V_{mp,ref}$)	35.4 V	26.2 V
Current at maximum power point at STC ($I_{mp,ref}$)	4.95 A	7.63 A
Maximum Power at STC at STC ($P_{max,ref}$)	175 W	200 W
Number of cells connected in series (N_s)	72	54
Temperature coefficient of $I_{sc,ref}$ (α)	0.8 mA/°C	3.654 mA/°C
Temperature coefficient of $V_{oc,ref}$ (β)	−145 mV/°C	−113.56 mV/°C
Temperature coefficient of $P_{max,ref}$ (γ)	−0.43%/°C	−0.47%/°C
Nominal operating cell temperature (T_{NOCT})	45 °C	45 °C

Base on the Eq. (10), $V_{t,ref}$ can be obtained as:

$$V_{t,ref} = \frac{\beta T_{ref} - V_{oc,ref}}{\frac{N_s T_{ref}\alpha}{I_{ph,ref}} - 3N_s - \frac{qE_g N_s}{KT_{ref}}} \tag{11}$$

3.1.2. Photo current I_{ph} at STC

At the short circuit point (0, I_{sc}): $V = 0$, $I = I_{sc,ref}$, Eq. (3) can thus be represented as:

$$I_{sc,ref} = I_{ph,ref} - I_{0,ref}\left[\exp\left(\frac{I_{sc,ref}\cdot R_{s,ref}}{N_s V_{t,ref}}\right) - 1\right] - \frac{R_{s,ref} I_{sc,ref}}{R_{p,ref}} \tag{12}$$

Because series resistance is very small, just a small part of the photo current flows into the diode and parallel resistance. Thus, the current that flows through the diode and parallel resistance can be neglected. Therefore, Eq. (12) can be simplified as Eq. (13).

$$I_{ph,ref} \approx I_{sc,ref} \tag{13}$$

3.1.3. Diode saturation current I_0 at STC

At the open circuit point (V_{oc}, 0): $I = 0$, $V = V_{oc,ref}$, which can be substitute into Eq. (3),

$$0 = I_{ph,ref} - I_{0,ref}\left[\exp\left(\frac{V_{oc,ref}}{N_s V_{t,ref}}\right) - 1\right] - \frac{V_{oc,ref}}{R_{p,ref}} \tag{14}$$

Because the exponential term exp ($V_{oc,ref}/N_s V_{t,ref}$) is much larger than 1 and fraction $V_{oc,ref}/R_{p,ref}$ is much smaller than $I_{ph,ref}$, the equation can be simplified as Eq. (15).

$$0 \approx I_{sc,ref} - I_{0,ref}\exp\left(\frac{V_{oc,ref}}{N_s V_{t,ref}}\right) \tag{15}$$

Therefore,

$$I_{0,ref} = I_{sc,ref}\exp\left(\frac{-V_{oc,ref}}{N_s V_{t,ref}}\right) \tag{16}$$

3.1.4. Parallel resistance R_p at STC

At the maximum power point (MPP), dP/dV is equal to zero. Because $P = VI$, the relationship can be given by:

$$\left.\frac{dV}{dI}\right|_{P=P_{mp,ref}} = -\frac{V_{mp,ref}}{I_{mp,ref}} \tag{17}$$

So

$$\frac{V_{mp,ref}}{I_{mp,ref}} = R_{s,ref} + \frac{N_s V_{t,ref} R_{p,ref}}{a_{ref} + (R_{s,ref} + R_{p,ref})I_{sc,ref} - V_{oc,ref}} \tag{18}$$

Because of $R_{p,ref} \gg R_{s,ref}$, the Eq. (18) can be simplified as:

$$R_{p,ref} = \frac{(V_{mp,ref} - I_{mp,ref}R_{s,ref})(V_{mp,ref} - N_s V_{t,ref})}{(V_{mp,ref} - I_{mp,ref}R_{s,ref})(I_{sc,ref} - I_{mp,ref}) - N_s V_{t,ref} I_{mp,ref}} \tag{19}$$

3.1.5. Series resistance R_s at STC

At the MPP (V_{mp}, I_{mp}): $I = I_{mp,ref}$ and $V = V_{mp,ref}$, Eq. (3) can be represented as Eq. (20) by substituting Eq. (19) into Eq. (3):

$$I_{mp,ref} = I_{ph,ref} - I_{0,ref}\left[\exp\left(\frac{V_{mp,ref} + I_{mp,ref}R_{s,ref}}{N_s V_{t,ref}}\right) - 1\right] - \frac{(V_{mp,ref} + I_{mp,ref}R_{s,ref})[(V_{mp,ref} - I_{mp,ref}R_{s,ref})(I_{sc,ref} - I_{mp,ref}) - N_s V_{t,ref} I_{mp,ref}]}{(V_{mp,ref} - I_{mp,ref}R_{s,ref})(V_{mp,ref} - N_s V_{t,ref})} \tag{20}$$

Now only one remaining unknown parameter, i.e. series resistance in Eq. (20). Therefore 'fzero' solver in the Matlab is employed to get the value of series resistance. This algorithm is a combination of bisection, inverse quadratic interpolation and secant methods and it is applied to find the zero of a one-dimensional continuous function around given initial value for researchers.

3.2. Parameter analyses under general conditions

After determining the reference parameters under STC using the mathematical model in the above section, the *I-V* curve and *P-V* curve of the PV module under STC can be easily obtained. Then it is significant to generalize the model to other general conditions with various solar irradiance and temperature. This section describes the method of related parameters through the dependence of temperature and irradiance including photocurrentI_{ph}, diode saturation current I_0, parallel resistance R_p, series resistance R_s, and diode thermal voltage V_t.

The photo currentI_{ph} is affected by both radiation and temperature and its modification equation is given by:

$$I_{ph} = \frac{G}{G_{ref}} I_{ph,ref}(1 + \alpha\cdot(T_c - T_{ref})) \tag{21}$$

where G_{ref} and T_{ref} is the radiation intensity (W/m^2) and cell temperature (K) under STC respectively, T_c is the actual solar cell temperature (K), G is the solar radiation (W/m^2), α is the temperature coefficient of the short circuit current (%/°C).

From the Eq. (9), diode saturation current I_0 depends only on temperature, expressing as below:

$$I_0 = I_{0,ref}\left(\frac{T_c}{T_{ref}}\right)^3 \exp\left[\frac{qE_g}{K}\left(\frac{1}{T_{ref}} - \frac{1}{T_c}\right)\right] \tag{22}$$

where E_g is the material band gap (eV) and K is Boltzmann's constant (1.381E−23 J/K).

A lot of studies (Celik and Acikgoz, 2007; De Soto et al., 2006; Ma et al., 2014b) have demonstrated that the series resistance R_s has no relationship with solar radiance and temperature. Therefore the series resistance R_s is kept constant in this study as below.

$$R_s = R_{s,ref} \tag{23}$$

where $R_{s,ref}$ is the series resistance under STC (Ω).

The value of parallel resistance R_p stands the leakage current in the p-n interface of the diode and the edges (Alam et al., 2015). It has been reported that the sensibility of the model to the value of the shunt resistance is quite slight (Bai et al., 2014; Tian et al., 2012), which means a fixed R_p does not affect the PV cell characters significantly. As a result, in this study R_p is taken as inversely proportional to the solar irradiance, such simplification has been adopted and validated in our previous study (Ma et al., 2014b,c):

$$R_p = \frac{G_{ref}}{G} R_{p,ref} \tag{24}$$

where $R_{p,ref}$ is the parallel resistance at STC (Ω), G_{ref} is the solar

radiance at STC (W/m^2), G is the general solar radiance (W/m^2).

The diode thermal voltage V_t is a linear function of temperature, so the modification equation for ideality factor at general condition can be expressed by (Ma et al., 2014b):

$$V_t = \frac{T_c}{T_{ref}} V_{t,ref} \tag{25}$$

where $T_{c,ref}$ and $V_{t,ref}$ are the cell temperature (K) and the diode thermal voltage (V) at STC, respectively.

The performance of PV module depends on the irradiance, wind velocity, and cell temperature. Cell temperature usually fluctuates frequently due to changes in the ambient temperature and irradiance. In this study, the T_{NOCT} is employed to estimate the PV cell temperature, which is shown as Eq. (26) (Tian et al., 2012).

$$T_c = T_a + \frac{T_{NOCT} - 20}{800} G \tag{26}$$

where T_a is the ambient temperature (K) and T_{NOCT} is the nominal operating cell temperature provided by the manufacturer (°C), G is the solar irradiation under general conditions (W/m^2).

3.3. Simulation process

The main purpose of the research is to predict PV power according to the weather data. The simulating process in Matlab is presented in a flow chart (Fig. 2).

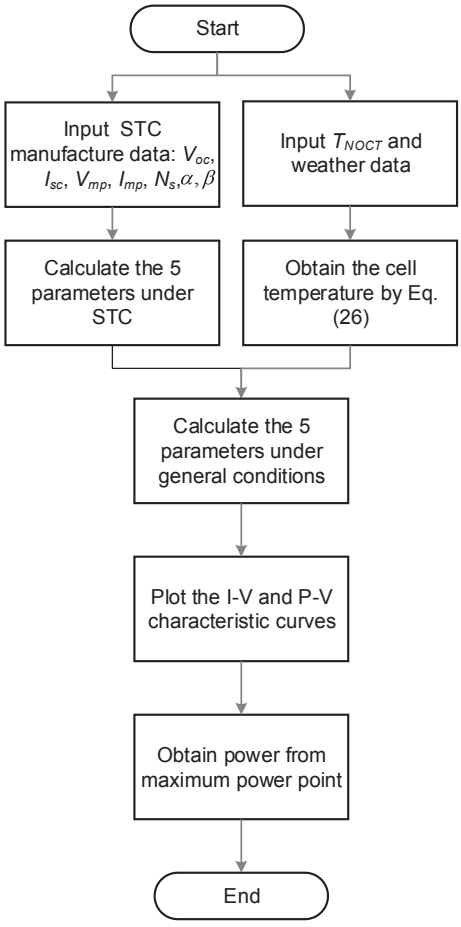

Fig. 2. Flow chart of the simulation process.

4. Results and discussion

4.1. Model verification and validation

4.1.1. Verification with other models

The mathematical model presented in Section 2 on the basis of Section 3 was programed in Matlab and then the related characteristic parameters of the proposed PV model under STC has been attained, and compared with the results from De Soto model (De Soto et al., 2006), PVsyst software, and our previous study, i.e. Ma model (Ma et al., 2014b). The results from the four models are summarized in Table 2.

As presented in Table 2, the photo-generated currents from the five models are appropriately the same regardless of cell type. There is an obvious difference for the diode saturation current, while the combination of series resistance and thermal voltage can make up the gap and guarantee the accuracy of the equation. However, the diode ideality factor of De Soto model derived from thermal voltage is less than 1, which is beyond the reasonable range. Table 2 also indicates that the parallel resistances from different models are very similar for monocrystalline silicon SQ175-PC, but they vary greatly for polycrystalline silicon STP200-18/Ub-1, which is acceptable for the purpose that the values of parallel resistance are huge enough to cause the leakage current minor and then the values have little impact on the character of *I-V* curves after all (Tian et al., 2012).

When calculated characteristic parameters are substituted into Eq. (3), the values at three characteristic points of the two different PV types ((V_{oc}, 0), (0, I_{sc}), (V_m, I_m)) can be obtained by inverse computation. Fig. 3 shows the deviation between the inversely calculated parameters and the data from the manufacturer.

For monocrystalline silicon SQ175-PC, our previous study (Ma model) shows the best agreement in $V_{oc,ref}$, $V_{mp,ref}$ and $I_{mp,ref}$ at MPP, whereas De Soto model and the proposed model have the best match in $I_{sc,ref}$, and $P_{max,ref}$, respectively. For Polycrystalline silicon STP200-18/Ub-1, our previous study shows the best agreement on $I_{sc,ref}$, while the best match on $V_{oc,ref}$, $V_{mp,ref}$, $I_{mp,ref}$ and $P_{max,ref}$ at MPP appears in the proposed model. Therefore, as a whole, the proposed model can be considered as the best model to simulate PV performance because it accounts for six best parameters out of ten.

According to the characteristic parameters under STC obtained in Table 2, the *I-V* and *P-V* curves under different cell temperature and the solar irradiance are studied to study the performance of the proposed model under general conditions. The *I-V* curves and *P-V* curves under different PV cell temperatures from 10 °C to 70 °C with irradiance at 1000 W/m^2 are illustrated in Fig. 4 (monocrystalline silicon SQ175-PC) and Fig. 5 (polycrystalline silicon STP200-18/Ub-1). The excellent matching from the proposed model, De Soto model and PVsyst software can be observed for the two different solar PV modules. A slight deviation exists from our previous study at the high cell temperature, but it is relatively small unless a good sight is equipped. That can be explained that the energy of band gap increases following the cell temperature and it becomes an obstacle to growing carrier concentration although the higher temperature leads to an increase in the intrinsic carrier concentration (Femia et al., 2012), and the minority carrier concentration increase as well, which reduces the open circuit voltage (Schwede et al., 2010).

Figs. 6 and 7 presents the *I-V* curves and *P-V* curves of monocrystalline silicon SQ175-PC and polycrystalline silicon STP200-18/Ub-1, respectively, in which solar radiation increases from 200 W/m^2 to 1000 W/m^2 with cell temperature of 25 °C. As presented in the figures, the difference for polycrystalline silicon PV is obviously smaller than that of the monocrystalline silicon PV. Besides, the four models represent a high degree of consistency at high irradiance while some deviations appear at low irradiance, especially for the monocrystalline silicon PV at the irradiance of 200 W/m^2. However, it is so tiny that it can be acceptable in most cases.

Based on above four figures, the model developed in this study

Table 2
Summary of characteristic parameters under STC using different methods.

Parameter	Monocrystalline silicon SQ175-PC				Polycrystalline silicon STP200-18/Ub-1			
	Ma	PVsyst	De Soto	This study	Ma	PVsyst	De Soto	This study
I_{ph}(A)	5.449	5.43	5.4568	5.43	8.123	8.12	8.12	8.12
I_0(A)	1.20E−09	2.00E−09	4.71E−11	2.91E−10	3.08E−09	1.01E−9	7.09E−10	7.67E−10
R_s(Ω)	0.6984	0.6500	0.8057	0.7043	0.3782	0.4000	0.4130	0.4055
R_p(Ω)	196.2	180.0	163.4	178.8	1031.6	2000.0	5000.0	2032.9
V_t(V)	0.0279	0.0285	0.0244	0.0262	0.0285	0.0271	0.0267	0.0268
n	1.086	1.110	0.948	1.019	1.1094	1.056	1.039	1.0426

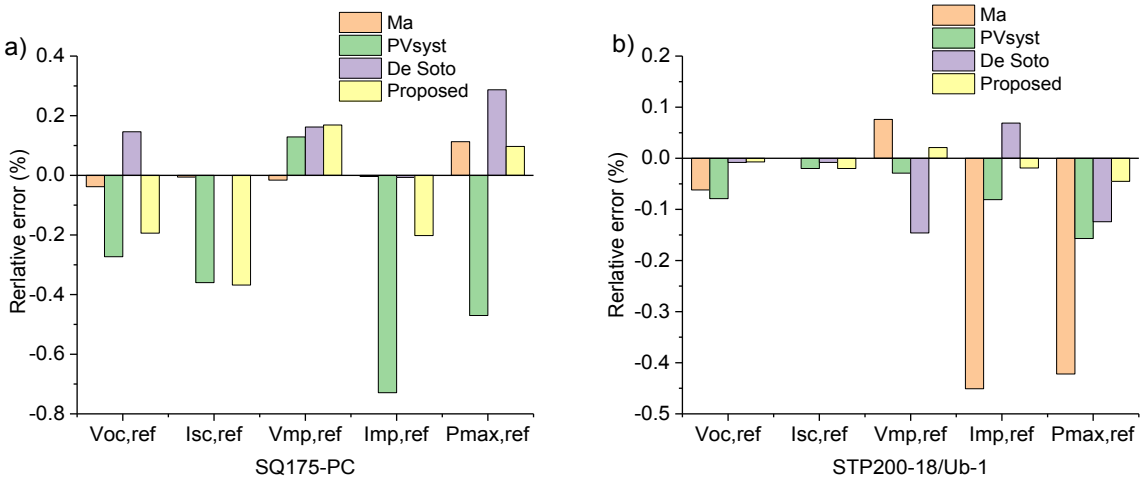

Fig. 3. The relative error of characteristic parameters: (a) SQ175-PC; (b) STP200-18/Ub-1.

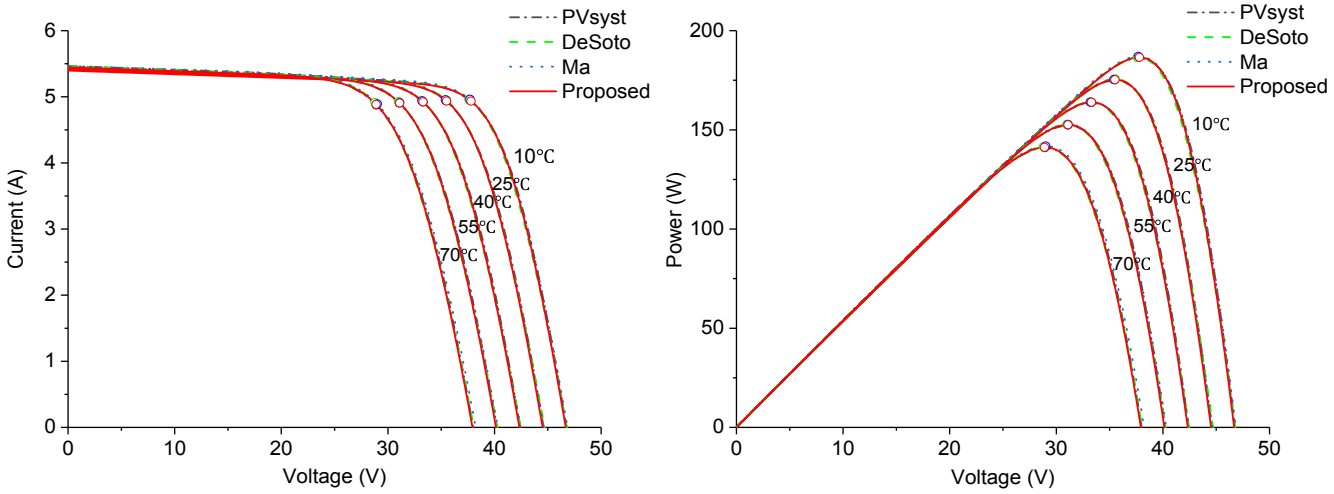

Fig. 4. The characteristic curves of SQ175-PC under different cell temperature (irradiance = 1000 W/m^2).

presents an excellent agreement with other widely used models, especially at the three characteristic points, in spite of the monocrystalline or polycrystalline silicon PV module. The deviation of maximum power from the proposed model and De Soto model which is commonly used and acceptable is within 2%, demonstrating that the mathematical model could be reliable for PV performance simulation and evaluations.

Besides the high accuracy of the model, the simplicity of the model is investigated, including simulation time, iterationsand function counts, as summarized in Table 3.

It can be seen that the simulation time of the proposed model is just half of other two models, because it only needs to solve four explicit equations in sequence and call a simple 'fzero' solver, instead of 'fsolve' which is employed in two other models to solve five or six nonlinear equations. Overall, it illustrates that the proposed model is handy and easily operated in various situations, and it is superior in evaluating the operationing performance of PV system.

4.1.2. Validation with experimental data

In order to further validate the model, some experimental tests have been conducted for the PV module SQ175-PC (Tossa et al., 2014) and STP200-18/Ub-1 (Ma et al., 2014c). Fig. 8 presents the simulated and measured *I-V* and *P-V* curves.

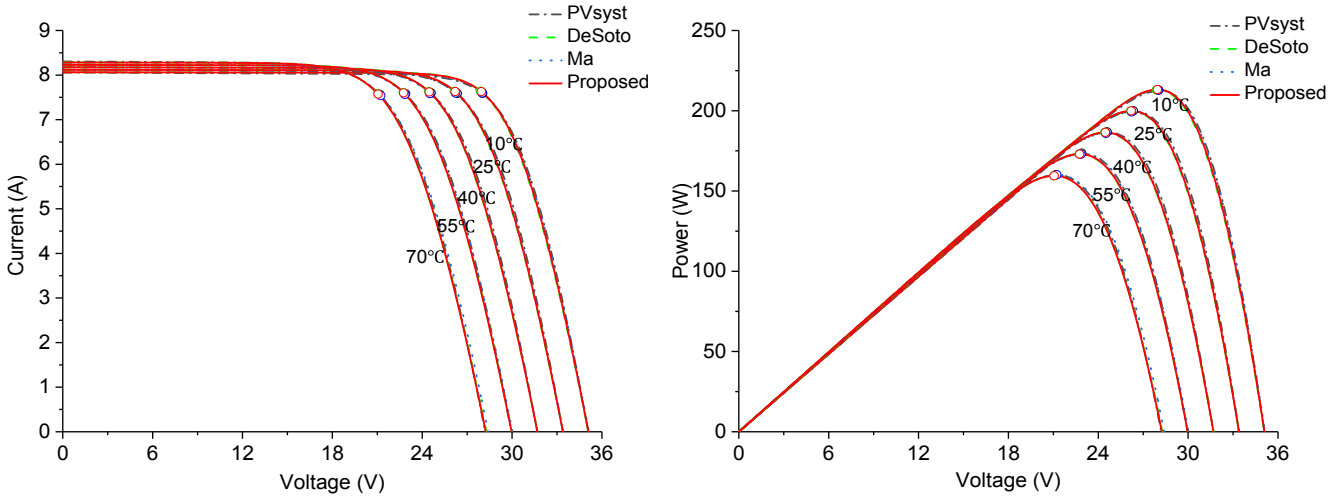

Fig. 5. The characteristic curves of STP200-18/Ub-1 under different cell temperature (irradiance = 1000 W/m^2).

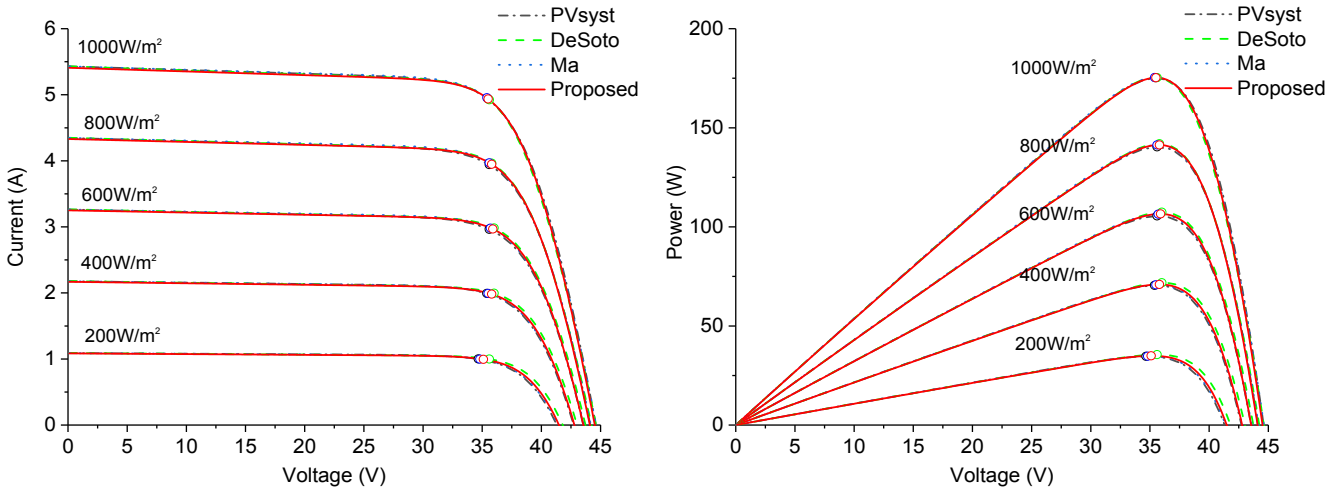

Fig. 6. The characteristic curves of SQ175-PC under different irradiance (cell temperature = 25 °C).

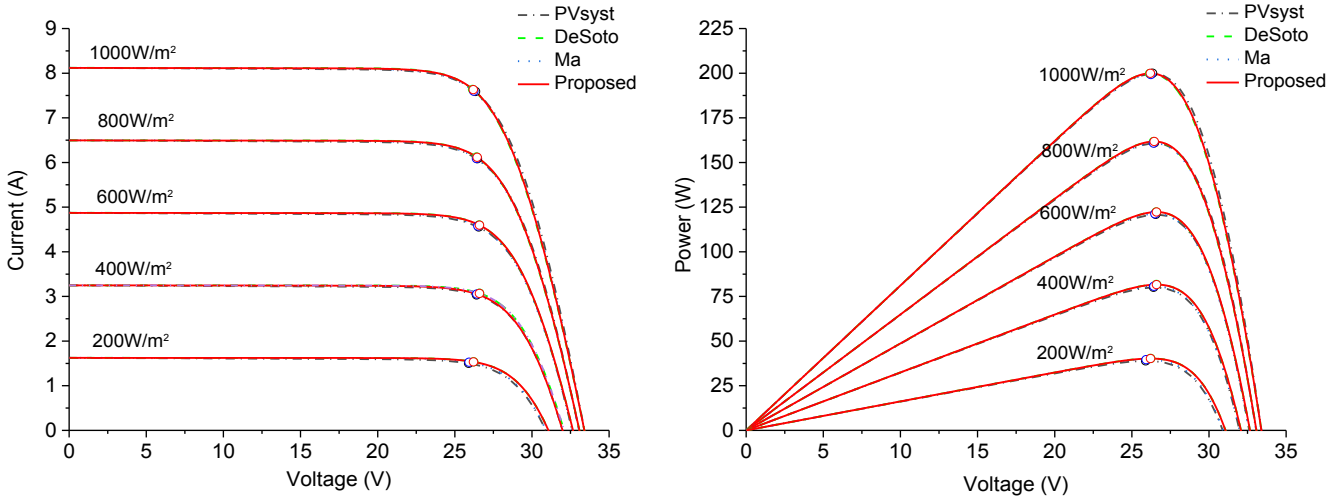

Fig. 7. The characteristic curves of STP200-18/Ub-1 under different irradiance (cell temperature = 25 °C).

For the differences between the simulated results and measured ones, it can be seen that the simulated curves match well with the measured curves for both PV types including maximum power output, and average relative errors for the two types of PV just reach 0.43% and 0.36%. While a minor difference can be seen for the STP200-18/Ub-1 PV module at the short circuit point due to the mismatch losses.

Table 3
Comparison of simplicity using different methods.

Item	Monocrystalline silicon SQ175-PC			Polycrystalline silicon STP200-18/Ub-1		
	Ma	De Soto	Proposed	Ma	De Soto	Proposed
Simulation time	40.1 ms	68.5 ms	26.2 ms	42.4 ms	50.1 ms	22.0 ms
Iterations	10	91	0	23	7	0
Function counts	66	595	33	158	79	13

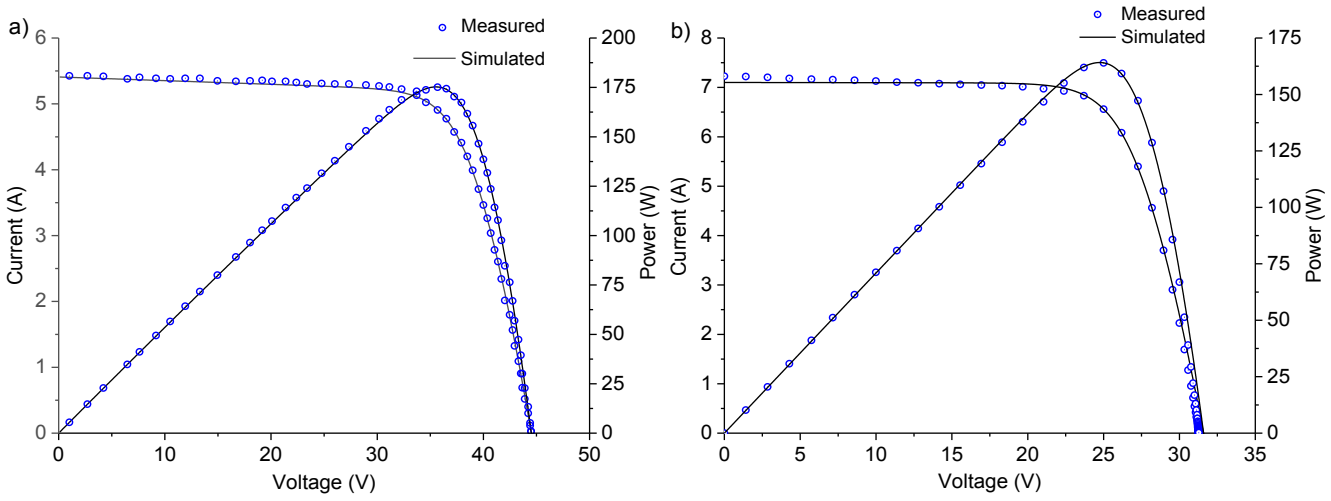

Fig. 8. The measured and simulated curves: (a) SQ175-PC; (b) STP200-18/Ub-1.

4.2. Short-term evaluations

After developing and validating the proposed model, it can be employed to predict PV system's power output under real weather conditions. Two typical weather conditions, i.e. sunny day and cloudy day, are taken as examples to compare simulated and measured power of the PV array. A real PV system involved in this study has been reported by our previous study (Ma et al., 2013, 2017). As shown in Fig. 9, the rated capacity of the PV array is 10.2 kW_p with three parallel strings of 17 modules connected in series. The solar PV module STP200-18/Ub-1 is used in this system and its key specification is listed in Table 1. All solar PV modules in this PV array are assumed to have the same working conditions under the specific weather condition (Ma et al., 2017). Also the PV array is supposed to work at its maximum power point because the mean efficiency of the PV inverter was examined as 97.1% in our previous study (Ma et al., 2013). Therefore the characteristic curves of the PV array was programmed and the power could be obtained at MPP by perturbing and observe algorithm (Bipu et al., 2015). The weather data and operation data were collected at the end of each 5 min (Ma et al., 2013). The pyranometer, purchased from EKO with high quality, is a well-known product and widely used in some scientific experimental tests for solar radiation measurement. The current, voltage, and ambient temperature were measured by PV inverter and thermometer. Table 4 (Pilougine et al., 2011) lists the method to assess the precisions of these data.

To quantify the accuracy of the proposed model, three performance indicators, i.e. the coefficient of determination (R^2) which measure the variation of simulation follows with collected data, the root mean square error (*RMSE*) which measures nonsystematic error, and the mean bias error (*MBE*) which measure systematic error, are employed in this study, they also have been already used in our previous study (Ma et al., 2014c). Their definitions are presented as Eqs. (27)–(29):

$$R^2 = 1 - \frac{\sum_{i=1}^{n}(y_i - f_i)^2}{\sum_{i=1}^{n}(y_i - \bar{y})^2} \tag{27}$$

$$RMSE = \sqrt{\frac{1}{n}\sum_{i=1}^{n}\left(\frac{f_i - y_i}{y_i}\right)^2} \tag{28}$$

$$MBE = \frac{1}{n}\sum_{i=1}^{n}\frac{f_i - y_i}{y_i} \tag{29}$$

where the measured data y_i is considered to be the 'real value', and the model simulated data f_i to be the 'calculated values'. The smaller *RMSE* and *MBE* values are, and the closer to 1 R^2 is, the better the simulated data matches with the measured data.

4.2.1. Sunny day case

The operating performance on 24th July 2011 was taken as an example for the performance analysis on a sunny day. Fig. 10 shows the irradiance, ambient temperature, and cell temperature on 24th July. The solar radiation intensity varies greatly from 5.29 W/m^2 to 944.75 W/m^2, averaging at 550 W/m^2. The ambient temperature changes from 24.74 °C to 38.68 °C, while the cell temperature fluctuates greatly from 24.91 °C to 60.51 °C. The peak difference between ambient temperature and cell temperature can reach to 29.52 °C, such high temperature can result in a negative impact of PV power generation by the rate of 0.47% per °C (Table 1).

The simulated and measured power output of the PV array versus time on the example day is presented in Fig. 11(a), illustrating clearly that the values of simulated power match the measured ones quite well. The simulated and measured power output increases when the solar radiation rises until noon. The simulated and measured power output curves reach the maximum point at noon and then reduce gradually because of a decreasing solar irradiance. The simulated results should be a little higher than the measured results without the consideration of power loss including mismatch loss, soiling loss and so on. Therefore, the simulated power is higher than the measured one in the morning and at noon. However, the power output is underestimated in the afternoon, which can be contributed to the strong wind on the island. Strong wind means good heat transfer conditions, causing the cell

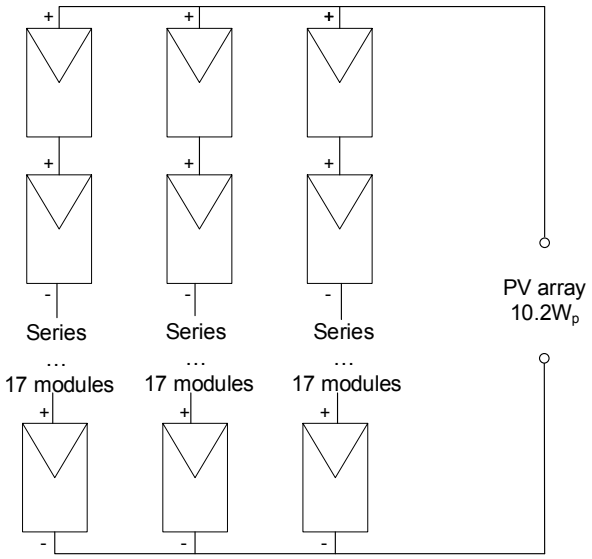

Fig. 9. Schematic diagram and experimental PV system.

Table 4
The specifications and precisions of measuring instruments.

Measuring instruments and model	Measured parameter	Absolute uncertainty
Pyranometer (EKO MS 602)	Irradiance (W/m^2)	7 μV/W/m^2
PV inverter (SMA Sunny Boy)	Current (A)	$\Delta I = 2\sqrt{8.6\times10^{-6}\cdot I^2 + 8.9\times10^{-8}\cdot\lvert I\rvert + 1.8\times10^{-6}}$
PV inverter (SMA Sunny Boy)	Voltage (V)	$\Delta U = 2\sqrt{7.1\times10^{-10}\cdot V^2 + 1.4\times10^{-7}\cdot\lvert V\rvert + 6.8\times10^{-6}}$
Thermometer (SENS0500)	Ambient temperature (°C)	$\Delta T_a = 2\sqrt{8.3\times10^{-6}\cdot T_a^2 + 10^{-3}\cdot\lvert T_a\rvert + 4.6\times10^{-1}}$

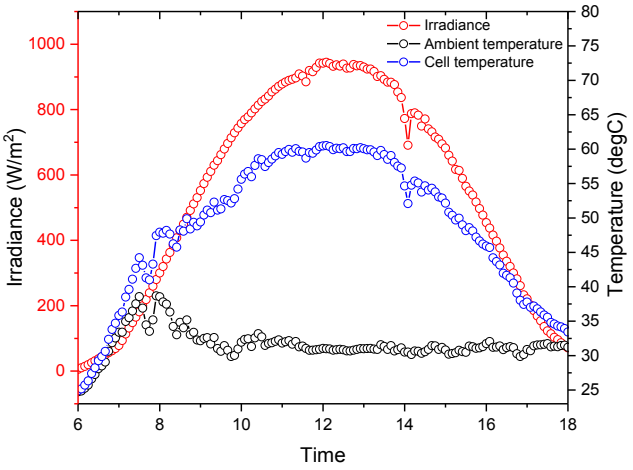

Fig. 10. The irradiance and temperature on a sunny day (24th July).

temperature lower and efficiency higher than the simulation results.

For the whole day, the average measured and simulated power output is 4.888 kW and 4.917 kW, respectively. To better evaluate the simulated result, the measured power versus simulated power was represented in Fig. 11(b). Obviously, the data is closely distributed along the y = x line (the slope of the fitting line is 0.9993), indicating that the simulated power possesses an excellent linear correlation with the measured power.

As a whole, the measured daily energy, simulated daily energy and performance indicators under sunny case are listed in Table 5, with the difference less than 1%. Besides, the performance indicator *RMSE* and *MBE* are also very small, which demonstrate the accuracy again of the developed mathematic model in this study.

4.2.2. Cloudy day case

In the case of a cloudy day on June 3rd, 2011, the irradiance fluctuates greatly from 20.93 W/m^2 to 998.73 W/m^2, averaging at 433.55 W/m^2 (Fig. 12). The ambient temperature changes slightly from 24.57 °C to 34.57 °C, while the cell temperature varies sharply from 25.22 °C to 61.55 °C because of the frequent change of solar radiation. The difference between ambient temperature and cell temperature peak at 31.21 °C.

On a cloudy day, the simulated and measured power curve of the PV array is demonstrated in Fig. 13. As presented in Fig. 13(a), the simulated power-output curve matches well with the measured curve. Some gaps are observed only at some peak points, which may result from the sensitivity of the pyranometer because of the rapid change of solar radiation intensity. Fig. 13(b) presents the linear relationship between the measured power and simulated power. From Fig. 13(b), it is obvious that all points are closely attached along the y = x line, and the slope of the fitting curve is 0.99263, meaning that there was a very good linear correlation between simulated power and the measured one.

Similarly, the measured yield, simulated yield and performance indicators under cloudy case are presented in Table 6. It is clearly seen that the measured yield is also very close to the simulated yield. The performance indicators *RMSE* and *MBE*, although, are a little higher than those in the sunny day, are acceptable for PV designers to estimate the energy yield on cloudy days.

4.3. Long-term evaluations

In order to check the long-term suitability of the model, the equipment for measure described in Section 4.2 was employed to attain the real operating data. The performance of the PV array in August and March as a representative of summer and spring, was used to evaluate the long-term performance. The irradiance was drawn by a box figure, as shown in Fig. 14.

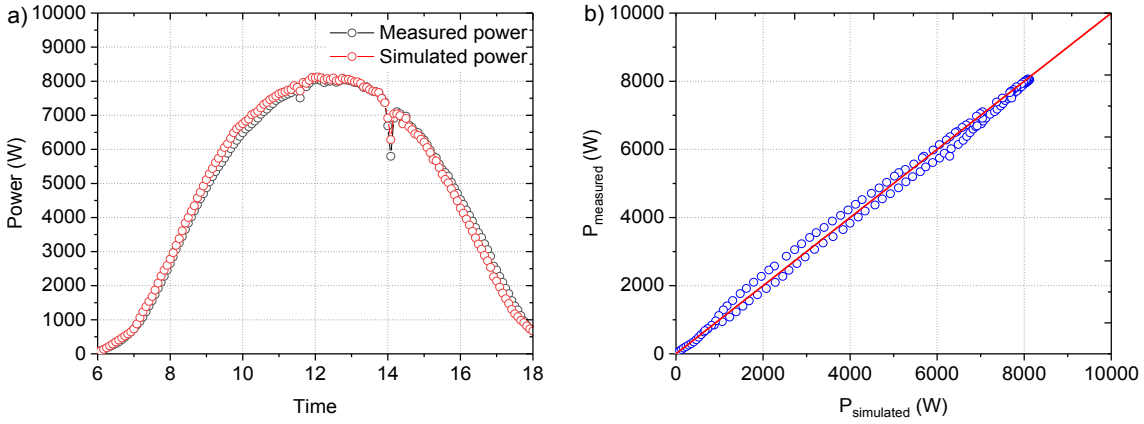

Fig. 11. The measured power and simulated power on a sunny day.

Table 5
Measured yield, simulated yield and performance statistic under a day sunny case.

Measured yield	Simulated yield	Error	R^2	*RMSE*	*MBE*
59.031 kW h	59.388 kW h	0.60%	0.9993	6.71%	0.73%

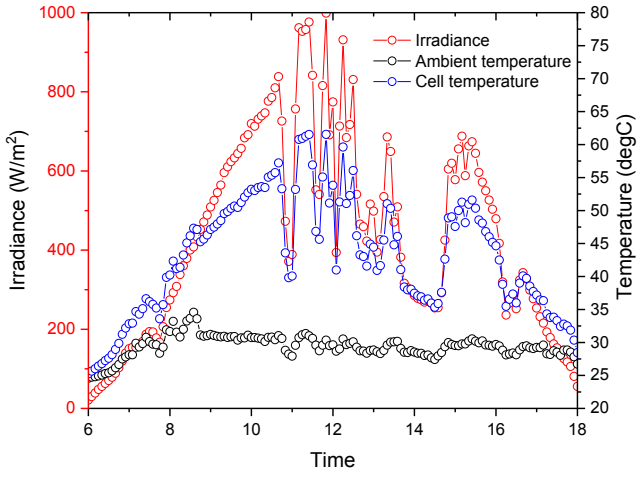

Fig. 12. The irradiance and temperature under a cloudy case.

Table 6
Measured yield, simulated yield and performance statistic under a cloudy case.

Measured yield	Simulated yield	Error	R^2	*RMSE*	*MBE*
48.837 kW h	48.309 kW h	−1.08%	0.99263	6.50%	0.82%

Most days in August can be considered as sunny days according to the solar radiance level. Several days such as 8th, 9th, 10th, and 17th can be taken as cloudy days. It can be observed that some irradiance values just on cloudy days emerge out of the 1.5 times interquartile range (1.5 IQR) to become outliers. Whereas the weather conditions in March are quite different. The values of irradiance for almost all days in March are lower than 200 W/m^2, and thus it could be called as a cloudy month. The outliers appear in August or in March due to the relatively long response time of the pyranometer, usually in the range of 5–25 s (Tossa et al., 2018). As a result, the pyranometer on cloudy days cannot catch up with the irradiance fluctuation, therefore there might some difference between real irradiation and the instant value collected by the pyranometer.

Figs. 15 and 16 presents the hourly simulated power and daily energy versus measured one, respectively. The simulated power fits the measured power very well whether in August or in March. The average deviation of simulated daily energy and measured one in August is just 2.9%, while 9.8% in March. It is noteworthy that the collected data is much lower than the simulated one, which can be explained that in the afternoon of 1st August, the load consumption from local inhabitants

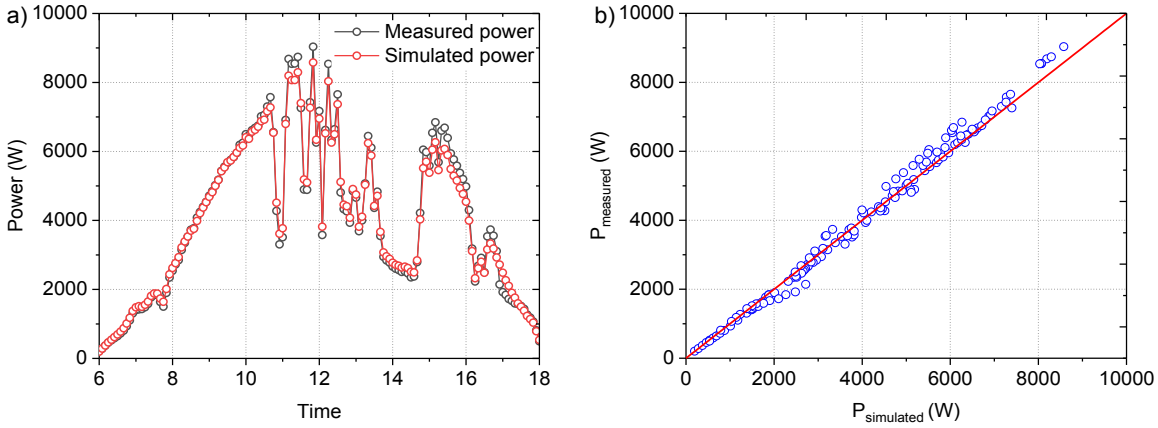

Fig. 13. The measured power and simulated power under a cloudy case.

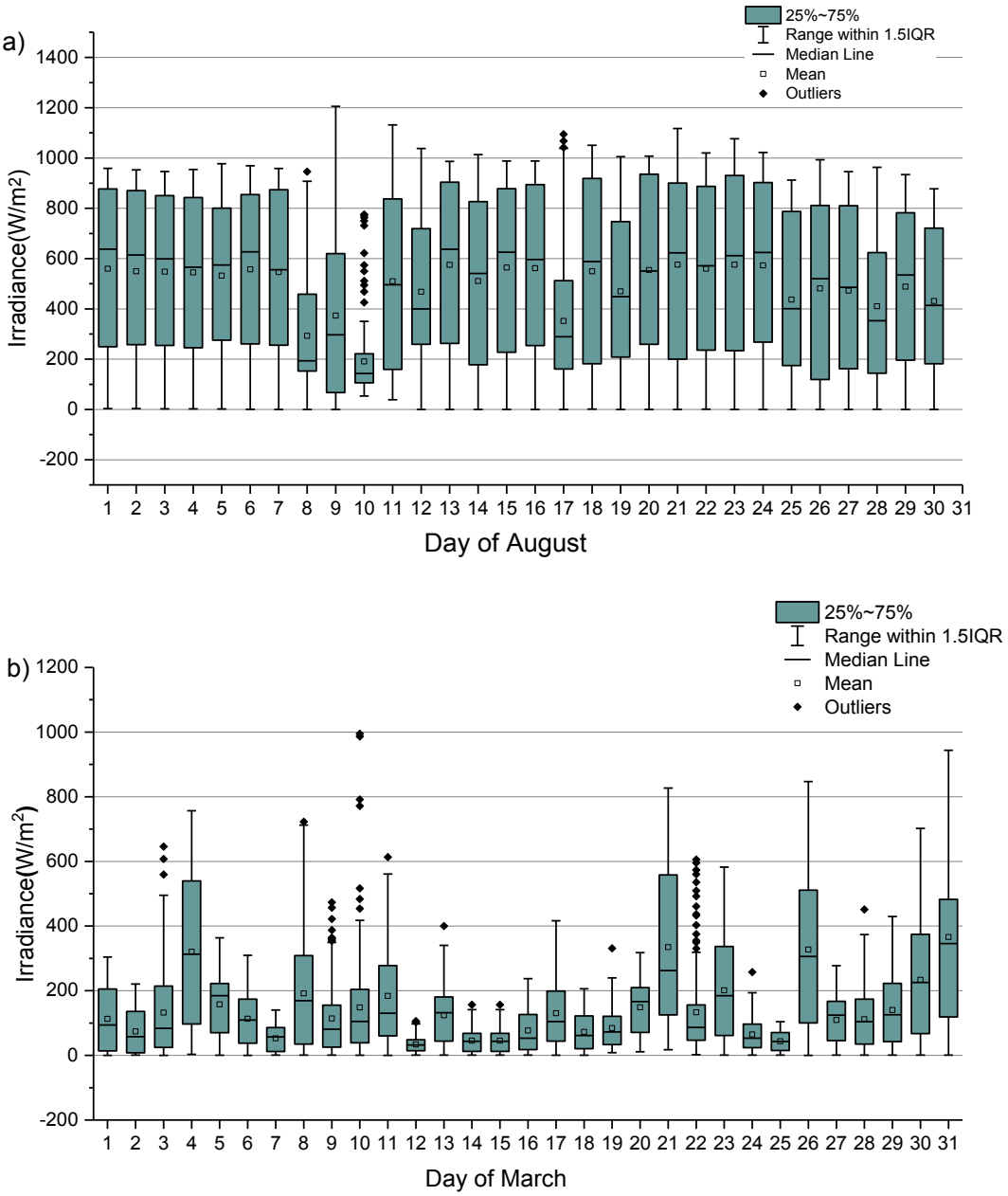

Fig. 14. Solar irradiance distribution during the month: (a) August; (b) March.

was much lower than potential yield from PV array and the state of charge (SOC) reached 100% and then some modules in the PV array were cut off (Ma et al., 2014c). As for the deviations, cloudy days in August and the cloudy month, the daily energy is overestimated especially in March, which might result from: (1) In fact, some outliers exist in August and more outliers in March due to the insensitive pyranometer, which cannot catch up with the irradiance fluctuation on cloudy days. (2) In addition, the spectral response of PV cells is very different from the pyranometer, which measures the almost full spectrum. On the cloudy days, long wave irradiation accounts for the majority, while it can be not absorbed by PV cells.

5. Conclusions

In this study, an improved and comprehensive mathematic model of PV modules using Matlab has been developed. This model presents a novel method of estimating performance for the PV modules revealing high accuracy and computational speed without complicated programming and multiple iterations.

With the basic data from manufacture, the *I-V* and *P-V* characteristics of a PV module at any operation conditions could be simulated. The simulation result from the proposed model presents excellent agreement with other commonly used models in literature for different types of PV modules. The proposed model is superior to other models in terms of computation speed. The simulated and experimental data under STC show consistency with each other and relative errors for two types of PV are just 0.43% and 0.36%. Furthermore, this model is employed to estimate the PV system power output under a sunny day and a cloudy day for short-term evaluations, and the relative error between the simulated energy and measured energy is 0.60% and −1.08%, respectively. August and March are chosen as examples for long-term evaluations of the PV system., and the deviation of simulated daily energy and measured one in August is just 2.9%, while 9.8% in March. The very good match between simulated and measured PV array

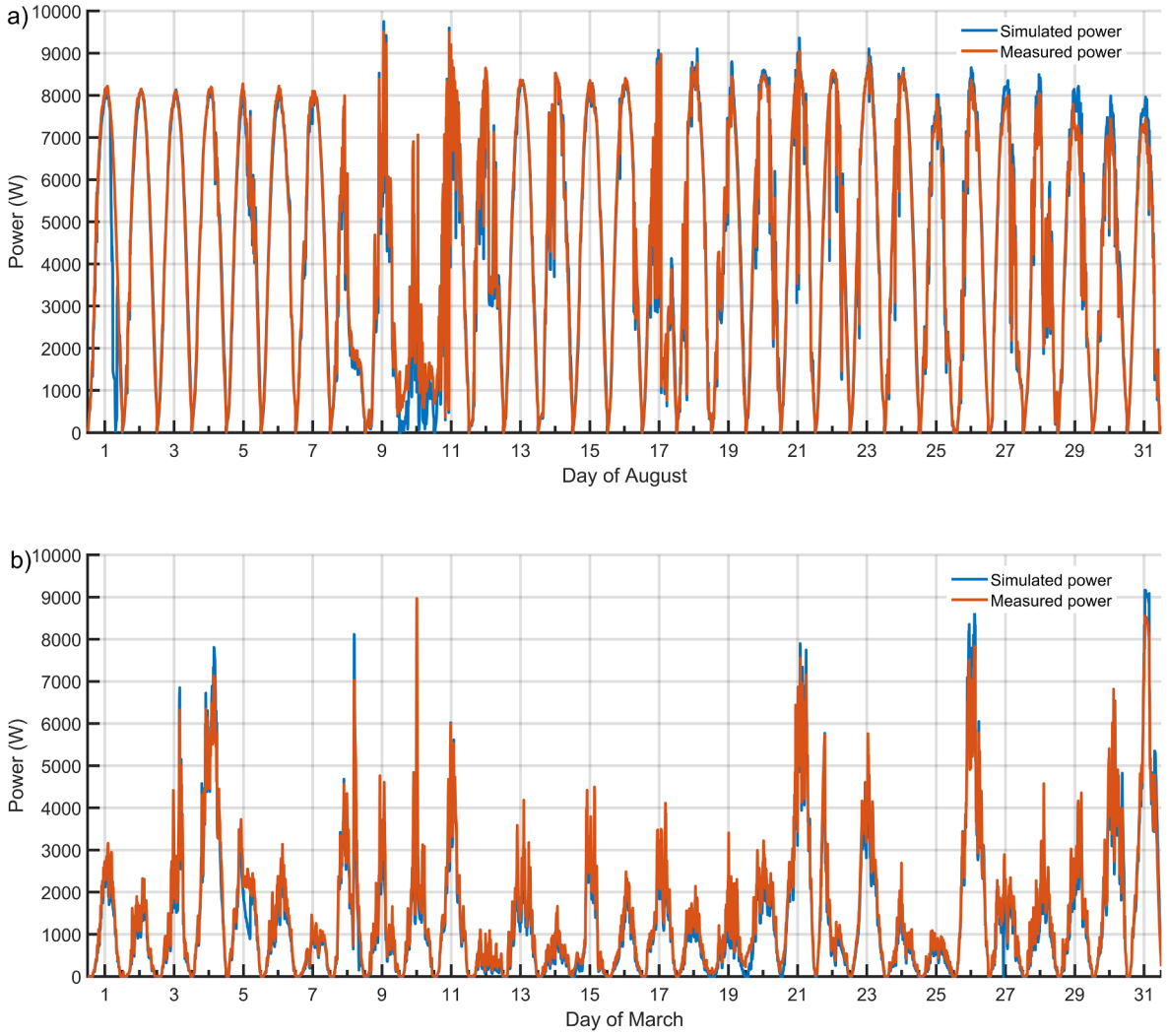

Fig. 15. The simulated power versus measured power during the month: (a) August; (b) March.

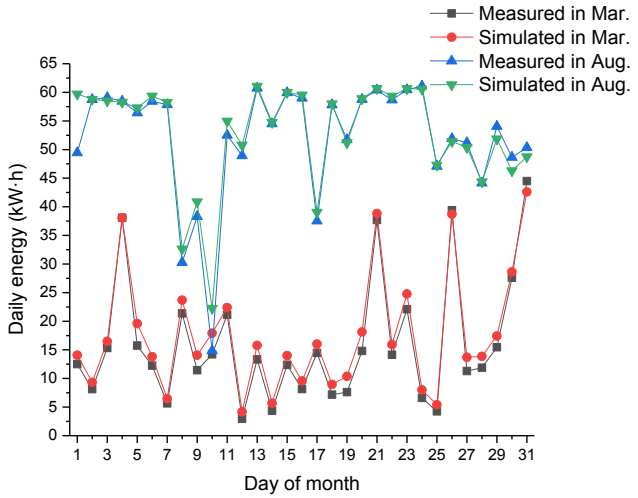

Fig. 16. Daily energy during the month.

power output in spite of weather conditions demonstrates the effectiveness of the proposed method for.

In all, this study presents a comprehensive PV simulation model and a novel determination solution, which is not only accurate but also quickly for PV designers and researchers to understand the actual relationship between current and voltage of PV system, and it can be further used to estimate its power output under real weather conditions, with the basic manufacturer template data.

Acknowledgments

The authors would appreciate the financial supports provided by Shanghai Pujiang Program through the Grant 18PJ1406000.

References

Alam, D.F., Yousri, D.A., Eteiba, M.B., 2015. Flower Pollination Algorithm based solar PV parameter estimation. Energy Convers. Manage. 101, 410–422.
Appels, R., Lefevre, B., Herteleer, B., Goverde, H., Beerten, A., Paesen, R., De Medts, K., Driesen, J., Poortmans, J., 2013. Effect of soiling on photovoltaic modules. Sol. Energy 96, 283–291.
Arefifar, S.A., Paz, F., Ordonez, M., 2017. Improving solar power PV plants using multivariate design optimization. IEEE J. Emerg. Selected Topics Power Electron. 5 (2), 638–650.
Awadallah, M.A., 2016. Variations of the bacterial foraging algorithm for the extraction of PV module parameters from nameplate data. Energy Convers. Manage. 113, 312–320.
Ayodele, T.R., Ogunjuyigbe, A.S.O., Ekoh, E.E., 2016. Evaluation of numerical algorithms used in extracting the parameters of a single-diode photovoltaic model. Sustain. Energy Technol. Assess. 13, 51–59.
Azizi, A., Logerais, P.-O., Omeiri, A., Amiar, A., Charki, A., Riou, O., Delaleux, F., Durastanti, J.-F., 2018. Impact of the aging of a photovoltaic module on the performance of a grid-connected system. Sol. Energy 174, 445–454.
Babu, B.C., Gurjar, S., 2014. A novel simplified two-diode model of photovoltaic (PV) module. IEEE J. Photovolt. 4 (4), 1156–1161.

Babu, J.S.K.A.C.S., 2012. Mathematical modeling and simulation of photovoltaic cell using Matlab-Simulink environment. Int. J. Electr. Comput. Eng. 2 (1), 26–34.
Bahaidarah, H.M.S., Baloch, A.A.B., Gandhidasan, P., 2016. Uniform cooling of photovoltaic panels: A review. Renew. Sustain. Energy Rev. 57, 1520–1544.
Bai, J., Liu, S., Hao, Y., Zhang, Z., Jiang, M., Zhang, Y., 2014. Development of a new compound method to extract the five parameters of PV modules. Energy Convers. Manage. 79 (2), 294–303.
Bana, S., Saini, R.P., 2016. A mathematical modeling framework to evaluate the performance of single diode and double diode based SPV systems. Energy Rep. 2, 171–187.
Bellia, H., Youcef, R., Fatima, M., 2014. A detailed modeling of photovoltaic module using MATLAB. NRIAG J. Astron. Geophys. 3 (1), 53–61.
Bipu, M.R.H., Chowdhury, S.M.S.M., Dautta, M., Nain, M.Z., Khan, S.I., 2015. Modeling and analysis of maximum power point tracking algorithms using MATLAB/Simulink. In: 2015 International Conference on Electrical Engineering and Information Communication Technology (ICEEICT), pp. 1–6.
Bouraiou, A., Hamouda, M., Chaker, A., Sadok, M., Mostefaoui, M., Lachtar, S., 2015. Modeling and simulation of photovoltaic module and array based on one and two diode model using Matlab/Simulink. Energy Procedia 74, 864–877.
Celik, A.N., Acikgoz, N., 2007. Modelling and experimental verification of the operating current of mono-crystalline photovoltaic modules using four- and five-parameter models. Appl. Energy 84 (1), 1–15.
Chaibi, Y., Salhi, M., El-jouni, A., Essadki, A., 2018. A new method to extract the equivalent circuit parameters of a photovoltaic panel. Sol. Energy 163, 376–386.
Chen, J., Huang, S., 2016. Simulation of photovoltaic module characteristics in arbitrary solar radiation and temperature. Laser Optoelectron. Progress 53 (2).
Chin, V.J., Salam, Z., Ishaque, K., 2015. Cell modelling and model parameters estimation techniques for photovoltaic simulator application: A review. Appl. Energy 154, 500–519.
Chin, V.J., Salam, Z., Ishaque, K., 2016. An accurate modelling of the two-diode model of PV module using a hybrid solution based on differential evolution. Energy Convers. Manage. 124, 42–50.
De Soto, W., Klein, S.A., Beckman, W.A., 2006. Improvement and validation of a model for photovoltaic array performance. Sol. Energy 80 (1), 78–88.
Dehghanzadeh, A., Farahani, G., Maboodi, M., 2017. A novel approximate explicit double-diode model of solar cells for use in simulation studies. Renew. Energy 103, 468–477.
Ding, M., Xu, Z., Wang, W., Wang, X., Song, Y., Chen, D., 2016. A review on China's large-scale PV integration: Progress, challenges and recommendations. Renew. Sustain. Energy Rev. 53, 639–652.
Doumane, R., Balistrou, M., Logerais, P.-O., Riou, O., Durastanti, J.-F., Charki, A., 2015. A Circuit-Based Approach to Simulate the Characteristics of a Silicon Photovoltaic Module With Aging.
Femia, N., Petrone, G., Spagnuolo, G., Vitelli, M., 2012. Power Electronics and Control Techniques for Maximum Energy Harvesting in Photovoltaic Systems (Femia, N. et al; 2013) [Book News].
Gökmen, N., Hu, W., Hou, P., Chen, Z., Sera, D., Spataru, S., 2016. Investigation of wind speed cooling effect on PV panels in windy locations. Renew. Energy 90, 283–290.
Goe, M., Gaustad, G., 2015. Estimating direct climate impacts of end-of-life solar photovoltaic recovery. Sol. Energy Mater. Sol. Cells.
Ibrahim, H., Anani, N., 2017. Evaluation of analytical methods for parameter extraction of PV modules. Energy Procedia 134, 69–78.
Ishaque, K., Salam, Z., Syafaruddin, 2011a. A comprehensive MATLAB Simulink PV system simulator with partial shading capability based on two-diode model. Sol. Energy 85 (9), 2217–2227.
Ishaque, K., Salam, Z., Taheri, H., Syafaruddin, 2011b. Modeling and simulation of photovoltaic (PV) system during partial shading based on a two-diode model. Simul. Model. Pract. Theory 19 (7), 1613–1626.
Jordehi, A.R., 2016. Parameter estimation of solar photovoltaic (PV) cells: A review. Renew. Sustain. Energy Rev. 61, 354–371.
Junnan, Y., Xiaoyuan, L., Wei, P., Fabian, W., Denise, L.M., 2018. Climate, air quality and human health benefits of various solar photovoltaic deployment scenarios in China in 2030. Environ. Res. Lett. 13 (6), 064002.
Khatib, T., Sopian, K., Kazem, H.A., 2013. Actual performance and characteristic of a grid connected photovoltaic power system in the tropics: A short term evaluation. Energy Convers. Manage. 71, 115–119.
Kimber, A., Mitchell, L., Nogradi, S., Wenger, H., 2007. The effect of soiling on large grid-connected photovoltaic systems in California and the Southwest Region of the United States. In: Conference Record of the 2006 IEEE 4th World Conference on Photovoltaic Energy Conversion, WCPEC-4, IEEE, pp. 2391–2395.
Kittisontirak, S., Bupi, A., Chinnavornrungsee, P., Sriprapha, K., Thajchayapong, P., Titiroongruang, W., 2016. An improved PV output forecasting model by using weight function: a case study in Cambodia. Int. J. Photoenergy 2016, 1–10.
Kou, Q., Klein, S.A., Beckman, W.A., 1998. A method for estimating the long-term performance of direct-coupled PV pumping systems. Sol. Energy 64 (1), 33–40.
Krismadinata, Rahim, N.A., Ping, H.W., Selvaraj, J., 2013. Photovoltaic Module Modeling using Simulink/Matlab. Procedia Environ. Sci. 17, 537–546.
Kumar, V., Shrivastava, R.L., Untawale, S.P., 2015. Solar energy: review of potential green & clean energy for coastal and offshore applications. Aquat. Procedia 4, 473–480.
Lim, L.H.I., Ye, Z., Ye, J., Yang, D., Du, H., 2015. A linear method to extract diode model parameters of solar panels from a single I-V curve. Renew. Energy 76, 135–142.
Ma, J., Guo, T., Lun, S., 2014d. An new explicit I–V model based on Chebyshev polynomials for two-diode model of photovoltaic modules. In: Proceedings of 2014 IEEE International Conference on Service Operations and Logistics, and Informatics, pp. 362–367.
Ma, T., Yang, H., Lu, L., 2013. Performance evaluation of a stand-alone photovoltaic system on an isolated island in Hong Kong. Appl. Energy 112, 663–672.
Ma, T., Yang, H., Lu, L., 2014a. Development of a model to simulate the performance characteristics of crystalline silicon photovoltaic modules/strings/arrays. Sol. Energy 100, 31–41.
Ma, T., Yang, H., Lu, L., 2014b. Development of a model to simulate the performance characteristics of crystalline silicon photovoltaic modules/strings/arrays. Sol. Energy 100 (2), 31–41.
Ma, T., Yang, H., Lu, L., 2014c. Solar photovoltaic system modeling and performance prediction. Renew. Sustain. Energy Rev. 36, 304–315.
Ma, T., Yang, H., Lu, L., 2016. Long term performance analysis of a standalone photovoltaic system under real conditions. Appl. Energy.
Ma, T., Yang, H., Lu, L., 2017. Long term performance analysis of a standalone photovoltaic system under real conditions. Appl. Energy 201 (Supplement C), 320–331.
Marco Tina, G., 2016. Simulation model of photovoltaic and photovoltaic/thermal module/string under nonuniform distribution of irradiance and temperature. J. Sol. Energy Eng. 139 (2).
Mejia, F.A., Kleissl, J., 2013. Soiling losses for solar photovoltaic systems in California. Sol. Energy 95, 357–363.
Navabi, R., Abedi, S., Hosseinian, S.H., Pal, R., 2015. On the fast convergence modeling and accurate calculation of PV output energy for operation and planning studies. Energy Convers. Manage. 89, 497–506.
Piliougine, M., Carretero, J., Mora-López, L., Sidrach-De-Cardona, M., 2011. Experimental system for current–voltage curve measurement of photovoltaic modules under outdoor conditions. Prog. Photovolt. Res. Appl. 19 (5), 591–602.
Kou, Q., Klein, S.A., Beckman, W.A., 1998. A method for estimating the long-term performance of direct-coupled PV pumping systems.
Reddy, S.R., Ebadian, M.A., Lin, C.X., 2015. A review of PV-T systems: Thermal management and efficiency with single phase cooling. Int. J. Heat Mass Transf. 91, 861–871.
Schwede, J.W., Bargatin, I., Riley, D.C., Hardin, B.E., Rosenthal, S.J., Sun, Y., Schmitt, F., Pianetta, P., Howe, R.T., Shen, Z.X., 2010. Photon-enhanced thermionic emission for solar concentrator systems. Nat. Mater. 9 (9), 762–767.
Shen, Y., Yao, W., Wen, J., He, H., 2018. Adaptive wide-area power oscillation damper design for photovoltaic plant considering delay compensation. IET Gener. Transm. Distrib. 11 (18), 4511–4519.
Silva, F.A., 2012. Power electronics and control techniques for maximum energy harvesting in photovoltaic systems (Femia, N. et al; 2013) [Book News]. Ind. Electron. Mag. IEEE 7 (3), 66–67.
Sun, L., Lu, L., Yang, H., 2012. Optimum design of shading-type building-integrated photovoltaic claddings with different surface azimuth angles. Appl. Energy 90, 233–240.
Tian, H., Mancilla-David, F., Ellis, K., Muljadi, E., Jenkins, P., 2012. A cell-to-module-to-array detailed model for photovoltaic panels. Sol. Energy 86 (9), 2695–2706.
Tossa, A.K., Soro, Y., Coulibaly, Y., Azoumah, Y., Migan-Dubois, A., Thiaw, L., Lishou, C., 2018. Artificial intelligence technique for estimating PV modules performance ratio under outdoor operating conditions. J. Renew. Sustain. Energy 10 (5), 053505.
Tossa, A.K., Soro, Y.M., Azoumah, Y., Yamegueu, D., 2014. A new approach to estimate the performance and energy productivity of photovoltaic modules in real operating conditions. Sol. Energy 110, 543–560.
Urrejola, E., Antonanzas, J., Ayala, P., Salgado, M., Ramírez-Sagner, G., Cortés, C., Pino, A., Escobar, R., 2016. Effect of soiling and sunlight exposure on the performance ratio of photovoltaic technologies in Santiago, Chile. Energy Convers. Manage. 114, 338–347.
Vimalarani, C., Kamaraj, N., 2015. Modeling and performance analysis of the solar photovoltaic cell model using Embedded MATLAB. Simulation 91 (3), 217–232.
Walker, G., 2014. Evaluating MPPT converter topologies using a Matlab PV Model. J. Electr. Electron. Eng.
Wang, Z., Ai, Q., Xie, D., Jiang, C., 2011. A research on shading and LCOE of building integrated photovoltaic, Asia-Pacific Power and Energy Engineering Conference, APPEEC. IEEE, pp. 1–4.
Watson, S., Bian, D., Sahraei, N., Winter, A.G.V., Buonassisi, T., Peters, I.M., 2018. Advantages of operation flexibility and load sizing for PV-powered system design. Sol. Energy 162, 132–139.
Yordanov, G.H., Midtgård, O.-M., Saetre, T.O., 2012. Series resistance determination and further characterization of c-Si PV modules. Renewable Energy 46 (5), 72–80.